JOURNAL OF MATERIALS SCIENCE 28 (1993) 3731–3740

The icosahedral to crystalline transformation in $Al_{51}Cu_{12.5}Li_{16.5}Mg_{20}$ melt-spun ribbons

P.E. DIEHL*, D.S. ZHOU, G.J. SHIFLET
Department of Materials Science, University of Virginia, Charlottesville, VA 22903, USA

The results of experiments on the icosahedral to crystalline transformation of melt-spun $Al_{51}Cu_{12.5}Li_{16.5}Mg_{20}$ are reported. The microstructural characteristics of the alloy, in all stages of the transformation, have been determined using a combination of transmission electron microscopy, X-ray diffraction and differential scanning calorimetry. The as-spun alloy consists of icosahedral grains with a low volume fraction of quenched-in crystallites. The quasilattice constant is calculated to be 0.505 nm. Upon annealing at 394 °C for 20 min, the icosahedral phase completely transforms to $Al_5Cu(Li, Mg)_3$ (a b c c phase), aluminium and a hexagonal phase. The orientation relationships and chemical compositions of all phases involved are established. Electron microscopy reveals planar defects in all the crystalline phases (except aluminium). The planar defects in the b c c phase are on {1 1 0} and {1 0 0}-type planes. Defects in the hexagonal phase are found to be on {0 0 0 1} and {11 $\bar{2}$ 0}-type planes.

1. Introduction

The discovery of quasicrystalline phases has resulted in much research activity in the field of crystallography. Following the publication of the first quasicrystal found, in aluminium manganese [1], numerous articles have appeared which report both experimental and theoretical studies done on over 60 systems which produce quasicrystalline structures. However, there are many questions yet unanswered, the most important of which is the position of the atoms in the quasicrystalline state.

The structural relationship between the quasicrystalline phases and its crystalline counterparts is of obvious importance, because it will enable information on the structure of the quasicrystalline phases to be deduced. Transformation behaviour between the quasicrystalline phases and the equilibrium phases has been studied in previous investigations [2–5].

The majority of alloys studied belong to the binary and ternary transition metal systems, most of which produce metastable quasicrystals. Their thermal instability makes it necessary to produce the quasicrystals by such methods as melt spinning. Relatively stable quasicrystals were found in the Al–Cu–Li and the Al–Cu–Li–Mg systems as precipitates at grain boundaries. The quasicrystal derived from the Al–Cu–Li system was the first stable quasicrystal discovered [6–10]. Icosahedral phases have been formed by conventional ingot casting (i.e. with low solidification rates) [6, 11–14] and by precipitation heat treatment of supersaturated solid solutions [15]. Hardy and Silcock [6] reported in 1955 on the isothermal section at 500 °C of the Al–Cu–Li system. They found the R-phase (Al_5CuLi_3) and the T2-phase (Al_6CuLi_3), which can now be identified as a b c c structure and the related icosahedral phase, respectively. The equilibrium structure was found to be isomorphous to $Mg_{32}(Al, Zn)_{49}$ [7], a structure with 61% of its 162 unit cell atoms having icosahedral symmetry. The structure of $Mg_{32}(Al, Zn)_{49}$, which was determined by Bergman *et al.* [16], was found to have a complex cubic layered structure with a lattice parameter of 1.416 nm. Each unit cell contains 162 atoms. The crystal structure was further refined in later investigations [17, 18].

It has been shown, however, that the exact positional parameters of the $Mg_{32}(Al, Zn)_{49}$ phase cannot be used for the R-phase [3, 19]. Shen [3] showed that the icosahedral phase and the b c c phase in Al–Cu–Li–(Mg) have a similar structure up to 2 nm, but their long-range order structure is quite different. The resulting structure essentially consists of double triacontahedra (DTs) in b c c positions [20]. To construct the related icosahedral phase a simple change in coordination numbers between DTs has been proposed [20]. X-ray diffraction data and measured transport properties indicate that the Al–Cu–Li icosahedral phase is one of the most ordered quasicrystals known.

Recently, there has been renewed interest in the Al–Cu–Li–(Mg) intermetallics, among other reasons because it has been shown that they have a strong relationship with their quasicrystalline counterparts [3, 20]. Evidence of this relationship is that both phases have the same chemical composition, they have definite orientation relationships, and the b c c phase grows at the expense of the icosahedral phase [20–22].

Grain boundary precipitates in Al–Cu–Li(–Mg–Zr) alloys have been identified as tetrahedrally close packed (T C P) phases [20, 23–25]. These

Present address: Center for Solid State Science, Arizona State University, Tempe, AZ 85287, USA.

0022–2461

intermetallic phases have a dense packing of slightly different size atoms with only tetrahedral interstices. The complete structure consists of tetrahedral bonding of atoms with coordination numbers 12, 14, 15 and/or 16. Tetrahedrally close packed phases generally consist of stacking polyhedra in space, the polyhedra being joined together by sharing along their triangles or hexagons. The T C P crystal structures, which are all layered compounds, were extensively studied by Frank and Kasper [7, 26, 27]. Intermetallics in dilute solid solutions of Al–Cu–Li–Mg systems have been studied by several research groups [25, 28–30]. Among the phases found are the C-phase [25, 28, 30], the Z-phase [29, 30], and the τ-phase [29, 30].

A feature common to many crystalline phases which are related to quasicrystals, seems to be that they have a high density of planar defects [20, 28–33], and the Al–Cu–Li–(Mg) system is no exception to this phenomenon. Because of the complex nature of the crystal structure, not much has been known about the defects in the crystalline phases, until recently. A better understanding of the defects will help elucidate the transformation from the quasicrystalline to crystalline state, and help in discovering the structure of the quasicrystals.

The primary aim of this work was to characterize fully the transformation of a pure quasicrystalline phase to its crystalline counterparts. Each of the phases present was examined using a variety of analytical techniques.

2. Experimental procedure

All alloys were prepared from high-purity (99.99 at %) constituent elements. The casting procedure was done in an induction furnace with an argon atmosphere. After this casting the ingot consisted of the crystalline Al–Cu–Li–Mg phase. The rapid solidification technique used was melt spinning. It was accomplished with a copper wheel of 20 cm diameter rotating at 4000 r.p.m. in an enclosed helium atmosphere and an ejection pressure of 150 kPa (22 p.s.i.). Cooling rates were of the order of 10^6 K s^{-1}. The resulting ribbons were between 2 and 3 mm wide, approximately 0.25 mm thick, and of varying length. The composition of the ribbons used in this study is given in Table I.

For heat treatment, the ribbons were encapsulated in quartz tubes evacuated to 10^{-5} torr (1 torr = 133.322 Pa) followed by back filling with $\frac{2}{3}$ atm argon. All heat treatments were done at 394°C in saltpots including several series ranging in time from 1–20 min (in 2–3 min intervals), followed by air cooling.

For conventional transmission electron microscopy (CTEM), a Philips 400T was used. The high-resolution electron microscopy (HREM) was done with a JEM-4000EX and the JEM atomic resolution microscope (ARM). An *in situ* hot-stage experiment was done, using a Kratos EM-1500. Energy dispersive spectroscopy (EDS) was employed for a semi-quantitative analysis of the phases present. Thin foils were obtained from the ribbons after the heat treatment and mounted on copper grids using epoxy. These samples were ion milled at low temperature, at 4 kV and at a 15° angle followed by final thinning at 8°.

Thermal analysis, using a Perkin–Elmer DSC-2, was carried out to determine the annealing times. The scanning speed employed was 40° min^{-1}, in the temperature range 25–650°C. A Siemens X-ray diffractometer, employing powder samples, provided qualitative information, as well as the lattice parameter data. The diffractometer used CuK-α radiation and operated at 40 kV and 20 mA.

TABLE I Composition (at %) of the melt-spun ribbons

Al	Cu	Li	Mg
51.0	12.5	16.5	20.0

3. Results and discussion

3.1. Electron microscopy analysis

3.1.1. Electron microscopy analysis of the as-spun ribbons

The melt-spun ribbons show the typical rosette microstructure of icosahedral crystals (Fig. 1). Grain sizes varied from 0.7–4.0 μm (diameter) in the thin foils studied, with most grains having a grain size around 1.5 μm. The grains, which all had the typical mottled appearance characteristic of the quasicrystalline phase, were identified by electron diffraction as having the icosahedral point group. All the diffraction patterns from the icosahedral grains displayed an interesting fine structure. Upon close inspection, individual

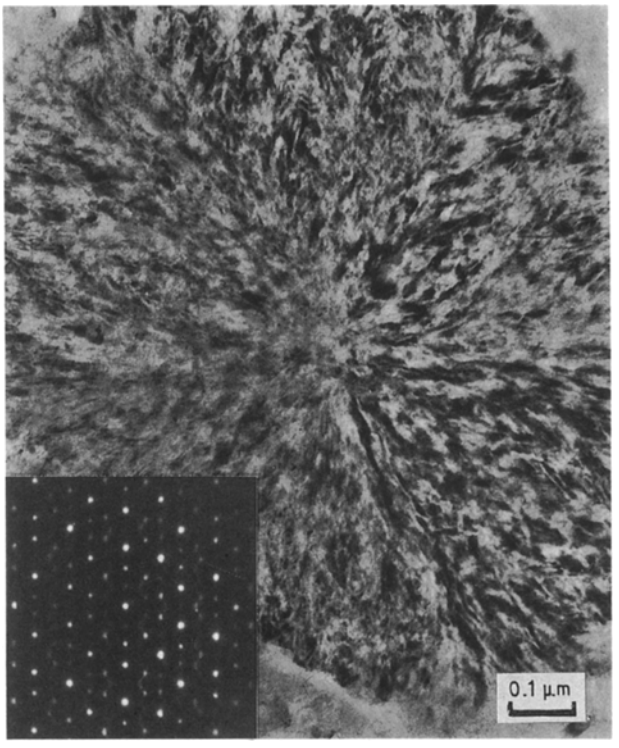

Figure 1 Bright-field micrograph of a typical icosahedral grain with a five-fold SAD.

spots in the pattern appeared as triangles, pentagons, and ellipsoids (inset, Fig. 1). It is assumed that each of these spots is composed of a number of diffraction events [34]. Previous investigations [35–38] have explained these spots as resulting from anisotropically quenched phason strains in the quasicrystals. There is no misalignment in the spots, as has been published in some previous studies.

Annealed ribbons which contained icosahedral grains still revealed this fine structure in the diffraction patterns, contrary to some previous publications which showed that upon annealing, defects may anneal out causing quasicrystals to relax, which will result in diffraction patterns with finer spots (see, for example, [4]). The shape of the spots did not change during annealing, which may confirm that phason strains are created during the growth of the quasicrystal, and are therefore frozen-in [39, 40]. The spots remained aligned after the annealing process, which could indicate that the icosahedral phase in this study is relatively stable compared with quasicrystals studied in other systems. The high degree of stability in this system has been confirmed by Shen [3], who studied the stability of a series of Al–Cu–Li–(Mg) alloys.

Crystallites, which can be identified by Moiré patterns (indicated by arrows in Fig. 2), were occasionally seen at high magnification in a few grains. This suggests that a low volume fraction of crystallites is present in the as-spun ribbons. These crystallites can be recognized by their contrast difference with the icosahedral phase, but cannot be further identified because of their small size.

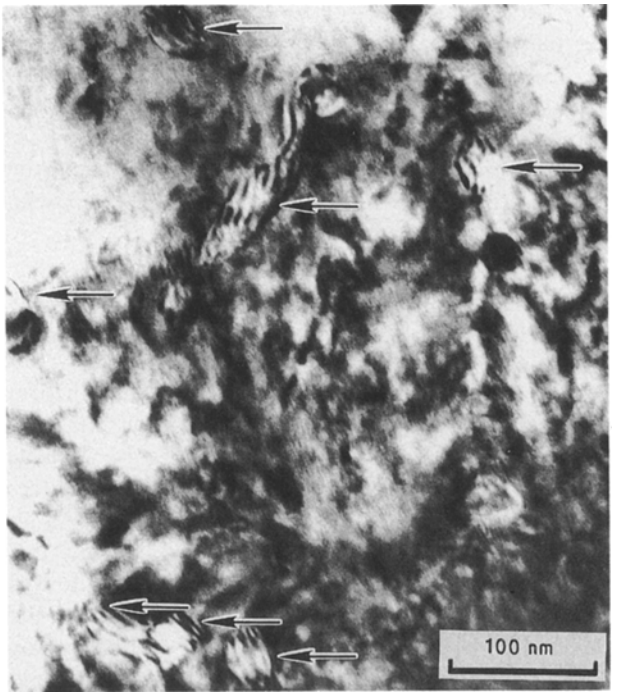

Figure 2 Bright-field micrograph of icosahedral grains, showing quenched-in crystallites.

A powder X-ray diffraction experiment was performed, and the resulting pattern was indexed using the Bancel *et al.* indexing scheme [41] (Fig. 3a). X-ray diffraction detected only the icosahedral phase. The quasilattice constant was determined to be 0.505 nm.

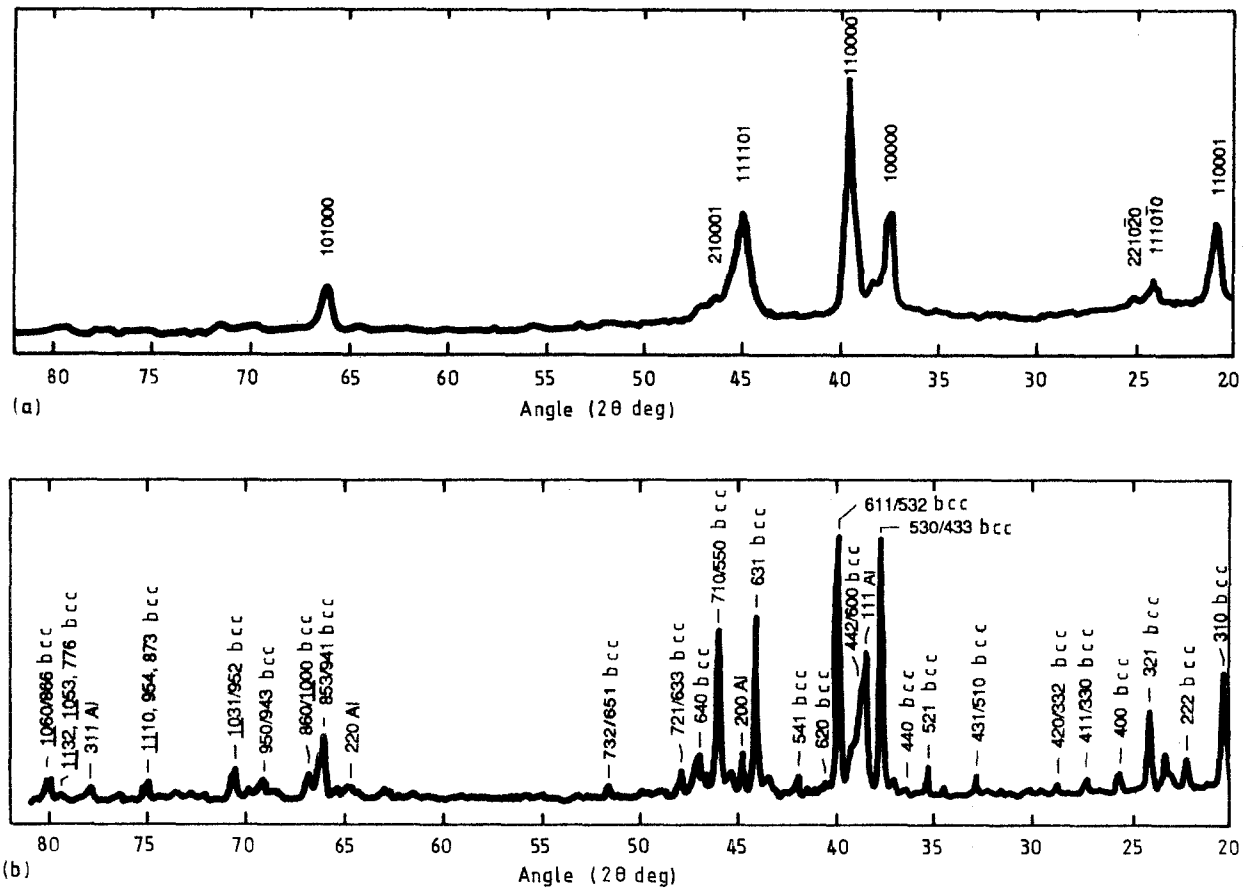

Figure 3 X-ray powder pattern of (a) the icosahedral phase, and (b) a completely transformed sample.

This value compared well to other quasicrystals having quasilattice constants between 0.507 and 0.518 nm [3, 4, 42]. The wave vectors and the diffraction intensities compared well to the T2 phase determined by Hardy and Silcock [6]. The diffraction peaks are broad, which can be explained as a result of the phason strains and/or the fine grain size [3, 35–38, 42].

3.1.2. Electron microscopy of the annealed ribbons

During the transformation, most of the icosahedral phase transforms to a complex crystalline phase. A typical grain of this phase is shown in Fig. 4a. Defects can be seen which are mainly parallel to three directions (indicated *A*, *B* and *C*). Fig. 4a also shows an aluminium crystal completely surrounded by this phase. Using a large-angle tilting experiment, this phase was determined to be the R-phase [20], with the chemical formula $Al_5Cu(Li, Mg)_3$. Fig. 4b and c show the [1 1 1] zone axis of the R-phase and the three-fold diffraction pattern of the icosahedral phase. These diffraction patterns were taken from two adjacent grains. In the crystalline diffraction pattern, six bright spots can be seen (indicated by arrows). The three-fold diffraction pattern of the icosahedral phase also contains six spots located at the same distance from the transmitted spot as the strong spots in the crystalline diffraction pattern. This suggests a close structural relationship between the icosahedral and the R-phase, and indicate the local icosahedral symmetry in this cubic phase.

Areas of the R-phase were imaged in the [0 0 1] and [1 1 1] directions. Fig. 5a–c show typical HREM micrographs of the linear defects in two orientations. All the defects can be explained by the shearing of planes [33, 43, 44]. The defects in Fig. 5a and b are the same $(1\bar{1}0)$ type, viewed along [1 1 1] and [0 0 1] directions, respectively, thus enabling a unique determination of the shear vectors [43]. The shear vectors of the 12 symmetrical equivalent $\{1\,1\,0\}$ shear planes were determined by Shiflet *et al.* [43]. The arrows in the figures indicate the shear planes [33, 43, 44]. Fig. 5c is taken along the [0 0 1] direction, and indicates a second type of shear (0 0 1) plane. Structural models of the shear planes, intersection areas and translation domains have been studied previously [43]. Yang *et al.* [44] have done a detailed study of the $\{1\,0\,0\}$ and $\{1\,1\,0\}$ type shear planes in this R-phase.

Other investigators [29, 30] have studied crushed crystals of Al_5CuLi_3 (R-phase) and also found $\{1\,1\,0\}$-type faults in the crystals. They explained these faults as a change of coordination number from 8 to 7 between triacontahedra. For perfect packing the triacontahedra overlap by eight neighbours along $\langle 1\,1\,1\rangle$ directions. They proposed that the R-phase propagates macroscopically as faulty periodic aggregates of atomic clusters with icosahedral symmetry.

The X-ray powder diffraction pattern (Fig. 3b) gives wave vectors and relative intensities which agree closely with the results of the R-phase determined by Hardy and Silcock [6]. All the peaks could be assigned either to the R-phase or to aluminium. The lattice parameter of the R-phase was determined to be 1.397 nm.

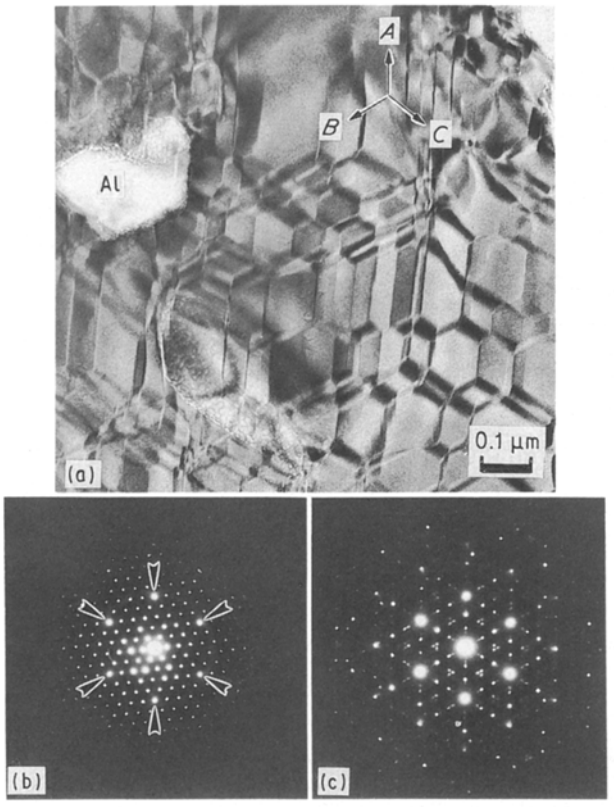

Figure 4 Bright-field image of network of defects in the R-phase ($B = [1\,1\,1]$) (a), SAD of R-phase [111] (b), and three-fold icosahedral phase (c), indicating the close structural relationship.

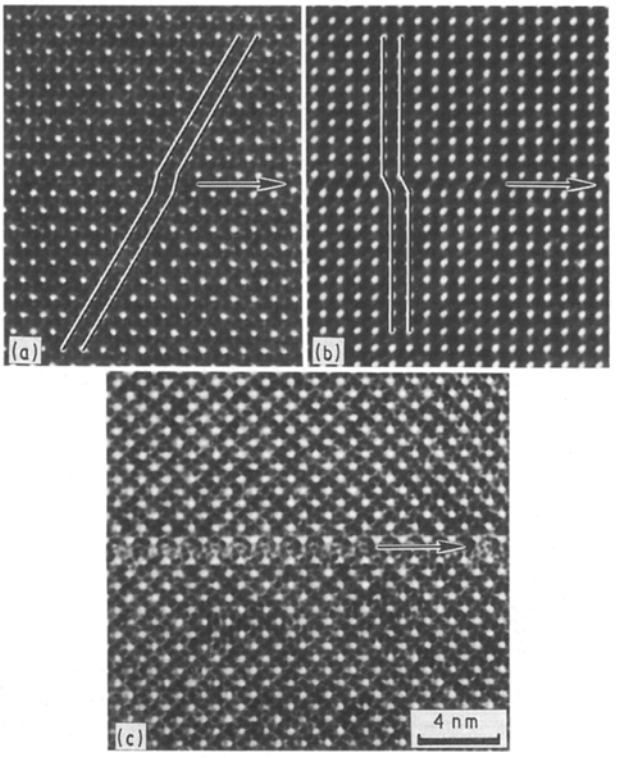

Figure 5 $(1\bar{1}0)$ fault in the R-phase viewed along (a) [1 1 1], (b) [0 0 1] and (c) [1 0 0] fault view along [0 0 1].

The cubic lattice constant, a_c, and the quasilattice constant, a_r, are related because the three-dimensional Penrose tiling can be generated by projections from a six-dimensional simple cubic lattice [35, 37, 45, 46]. Using a formula given by Audier *et al.* [20], the value of a_c was found to be 1.390 nm. This value corresponds closely to the value obtained by X-ray diffraction (i.e. 1.397 nm). Audier *et al.* [30] determined the cubic lattice constant to be 1.39056 nm, agreeing with the value found here.

The presence of aluminium, which was found in every sample that was heat treated, was confirmed by SAED and EDS. Fig. 4a shows an area of aluminium in a sample that was heat treated for 20 min at 394 °C.

In addition to the R-phase and aluminium, a hexagonal phase was observed. A bright-field image of this new phase surrounded by grains of the R-phase is shown in Fig. 6a. The image reveals linear defects which seem to extend throughout the grain. The Bravais lattice of this second phase, determined by large-angle tilting experiments (Fig. 6b–d), was found to be hexagonal. The lattice parameters were determined to be $a \approx 1.39$ nm and $c \approx 2.78$ nm.

The $1\,1\,\bar{2}\,0$ diffraction pattern in Fig. 6d shows ten strong spots, thus revealing a pseudo five-fold symmetry in this hexagonal diffraction pattern, indicating a close structural relationship with the icosahedral phase. This suggests a local icosahedral symmetry. Except for the Al–Fe–Si system [47], this result would indicate the only known icosahedral–hexagonal relationship.

Audier *et al.* [30] have reported a hexagonal phase (designated Z-phase) for which the a lattice parameter was equal to the b c c R-phase. The lattice parameter was determined to be $a = 1.403$ nm, $c = 2a$, and the space group was determined to be $P6_3/mmc$. All the evidence in the present experiment shows that the hexagonal phase found here is the Z-phase reported by Audier *et al.* In HREM pictures the Z-phase was shown to have a layered structure. A model for this phase was also proposed, namely the Z- and R-phase similarity in atomic arrangement led to the suggestion that the Z-phase could be constructed by connecting triacontahedra at their faces [30].

An HREM image of the Z-phase (along the $[1\,1\,\bar{2}\,0]$ direction) is shown in Fig. 7. Faults are found on

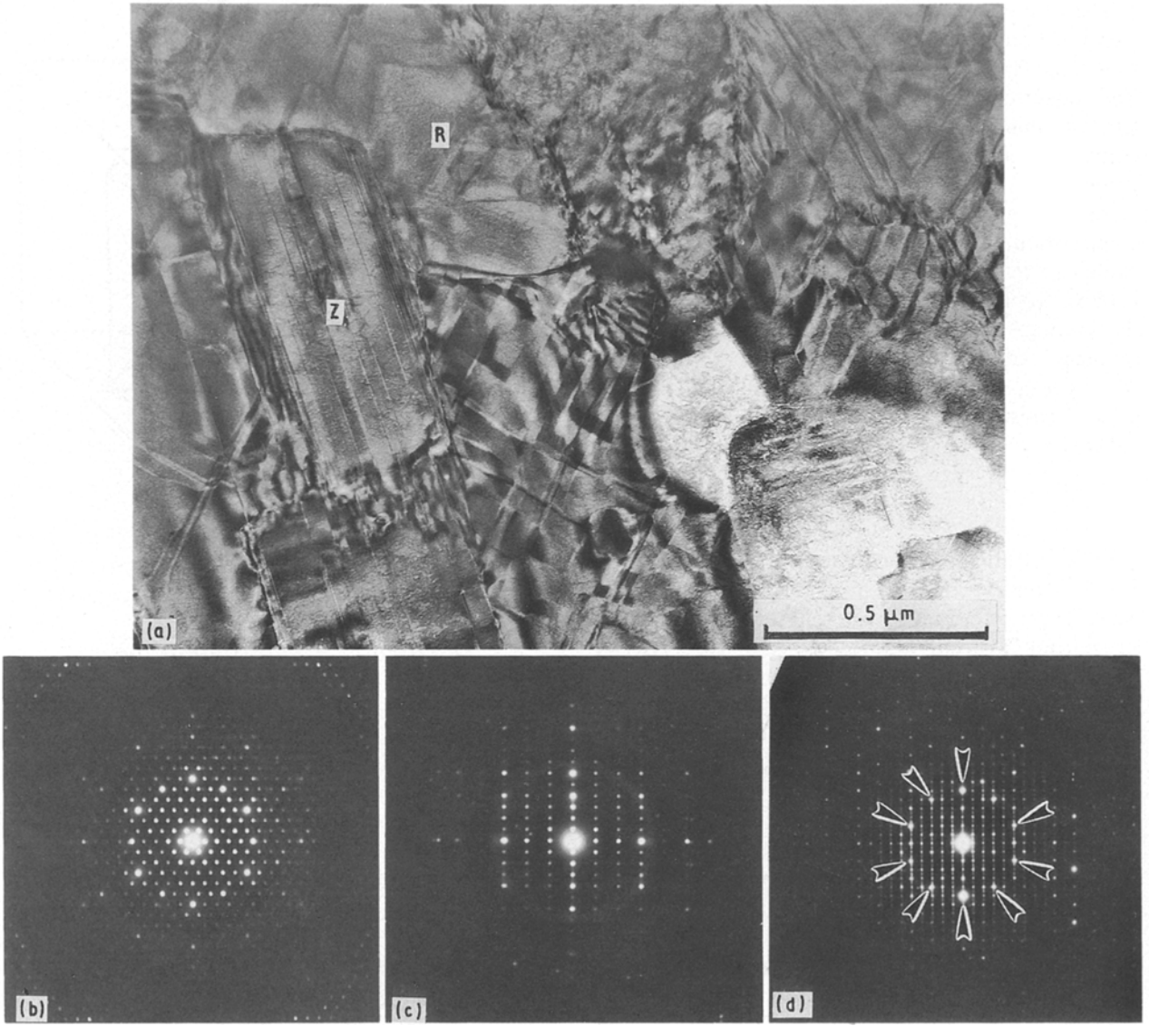

Figure 6 (a) Z-phase surrounded by R grains (b) [0 0 0 1] SAD pattern (c) $[0\,1\,\bar{1}\,0]$ SAD pattern, and (d) $[1\,1\,\bar{2}\,0]$ SAD pattern (with pseudo five-fold symmetry).

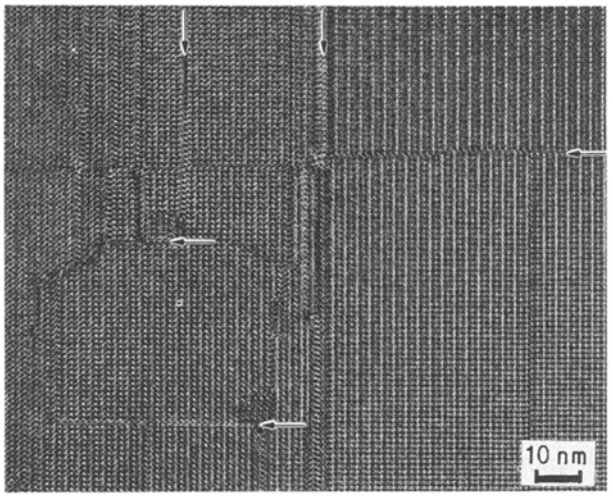

Figure 7 HREM image of the Z-phase along the [1 1 $\bar{2}$ 0] axis, showing defects mainly on (0 0 0 1) and (1 1 $\bar{2}$ 0) planes.

(0 0 0 1) and (1 1 $\bar{2}$ 0) planes (indicated by arrows). In some of the diffraction patterns (especially the (1 1 $\bar{2}$ 0) type, see Fig. 6d) continuous streaking can be seen which is due to the major faults and further confirms that faults lie on {0 0 0 1} type planes.

The results of EDS spectra are shown in Table II. Compositionally there is a significant difference between the Z-phase and the R- or icosahedral phase. The copper content of the hexagonal phase was 7.2% less than that of the two other phases. The aluminium content was found to be 6.6% higher than that of the icosahedral and R-phase. These chemistry results seem to suggest that this hexagonal phase is not compositionally related to the icosahedral phase. Audier *et al.* [30] determined the composition of the Z-phase to be $Al_{0.59}Cu_{0.05}Li_{0.26}Mg_{0.10}$. Ignoring the lithium, and normalizing the other atomic percentages transforms the Z-phase formula to $Al_{0.80}Cu_{0.07}Mg_{0.14}$. This result significantly differs from the results presented in our study, which may indicate a wide range of compositions for this phase.

TABLE II Composition (at %) of phases from EDS data

	Al	Cu	Mg
As-spun ribbon	61.08	14.97	23.95
Icosahedral phase	60.09	17.27	22.64
FK (R) phase	56.95	19.98	23.07
Hexagonal (Z) phase	63.55	12.78	23.67

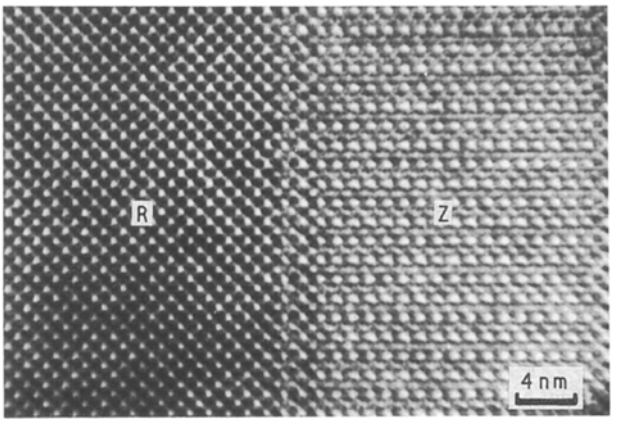

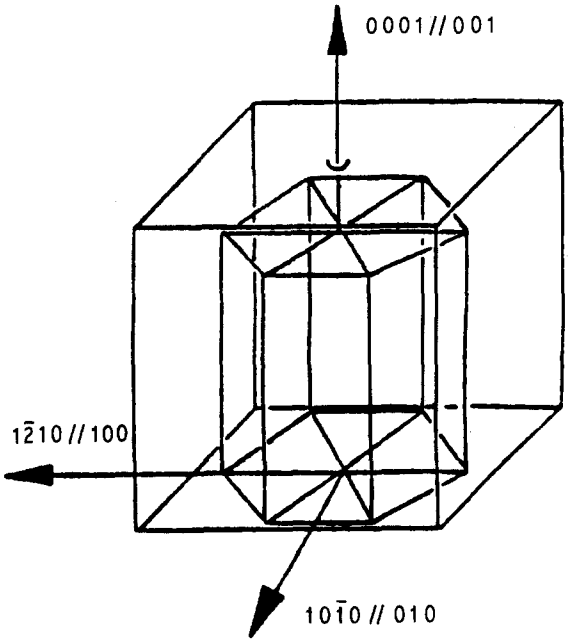

Figure 8 Interface between the R and Z-phases.

3.2. Orientation relationships

The orientation relationships between the various phases were determined by taking several SAED patterns from adjacent grains, and analysing HREM micrographs of interfaces. The orientation relationships can be best described by visualizing inscribed polyhedra (in this case icosahedra, cubes and hexagons).

3.2.1. Orientation relationship of the R- and Z-phases

Fig. 8 is a structure image of an interface between the two phases viewed along [1 0 0] of the R-phase and [1 1 $\bar{2}$ 0] of the Z-phase. The orientation relationship is described as follows: [0 0 1] || [0 0 0 1] and (0 1 0) || (1 0 $\bar{1}$ 0) (see inset of inscribed polyhedra in Fig. 8).

3.2.2. Orientation relationship of the R- and the icosahedral phase

Fig. 9 shows the R-icosahedral (I) interface. The cubic [1 0 0] zone axes were found to be parallel to the icosahedral two-fold axes and four of the three-fold icosahedral axes were found to be parallel to the cubic [1 1 1] directions. In Fig. 9 a [1 1 1] zone axis was found to be parallel to the three-fold icosahedral zone axis. An icosahedron inscribed in a cube represents the proposed orientation relationship of the icosahedral phase and the R phase [30]. The reference cube represents the major [0 0 1] axes of the cubic phase. The cube and the icosahedron are oriented so that one of the three two-fold axes of the icosahedron is fixed with the [0 0 1] zone axis. The set of two-fold icosahedral axes are lying at right angles to the [0 0 1] and

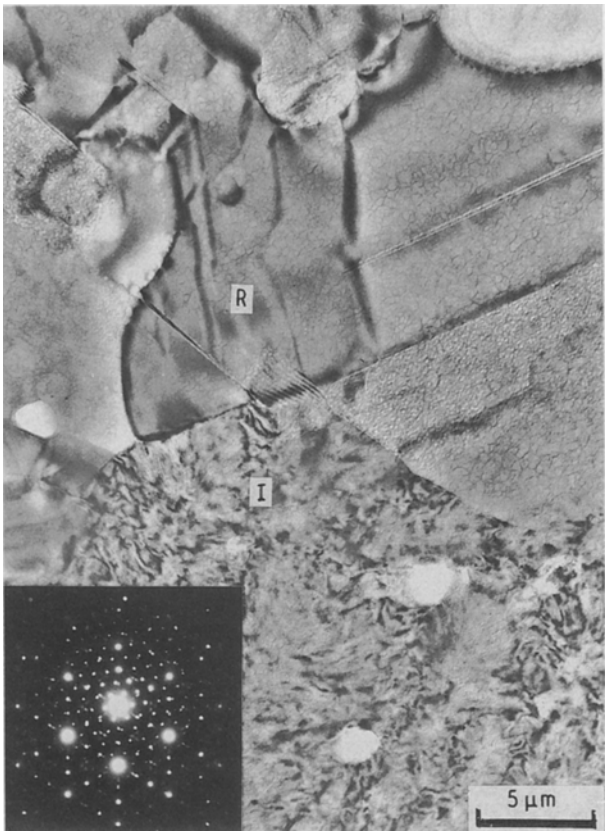

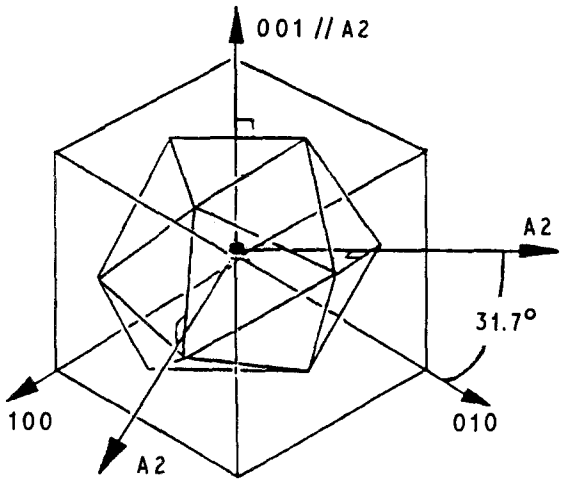

Figure 9 Icosahedral–R interface and SAD pattern showing the orientation relationship.

are rotated exactly 31.7° from the corresponding cube axes [0 1 0] and [1 0 0]. The resulting orientation relationships are: $[1\,0\,0] \| [A_2]$, $[\tau^2\,0\,1] \| [A_3]$, $[1\,0\,\tau] \| [A_5]$ and $[1\,\tau\,0] \| [A_5]$ (see inset of inscribed polyhedra in Fig. 9).

For the Al–Li–Cu system the orientation of the icosahedral phase and R-phase also fit the same orientation between a cube and an icosahedron (three-fold axes are in correspondence and the two-fold axis is parallel to the 1 0 0 axis of the cube) [25, 48]. This relationship was also reported between the b c c phase and the icosahedral phase in solid solutions of the Al–Cu–Li–Mg system [20] and in the Al–Mn–Si system [49].

3.2.3. Orientation relationship of the hexagonal and the icosahedral phase

It was very rare to encounter an interface of an icosahedral and hexagonal grain in any of the annealed ribbons studied. Fig. 10 shows this unique situation. The two-fold SAED pattern of the icosahedral was found to be parallel to the $1\,\bar{2}\,1\,0$ axis of the hexagonal phase (Fig. 10). Using this information, combined with the finding that some of the $1\,\bar{2}\,1\,0$-type SAED patterns show pseudo five-fold symmetry, leads to the following suggested orientation relationship. Four vertices, with five-fold symmetry, in the icosahedron, lie on a plane which is parallel to the 0 0 0 1 plane of the hexagon. As a result, two $1\,\bar{2}\,1\,0$-type axes are parallel to two five-fold icosahedral axes (see inset of inscribed polyhedra in Fig. 10). The five-fold axis almost coincides with the $1\,\bar{2}\,1\,0$-type axis, thus resulting in the pseudo five-fold symmetry observed in some of the $1\,\bar{2}\,1\,0$-type SAED patterns. This is the first reported orientation relationship between the Z-phase and the icosahedral phase.

By combining the results of Section 3.2, a self consistency in the orientation relationships between any of the three phases is evident.

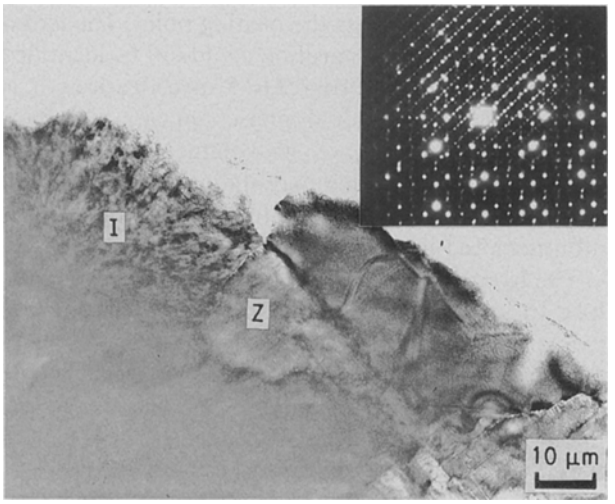

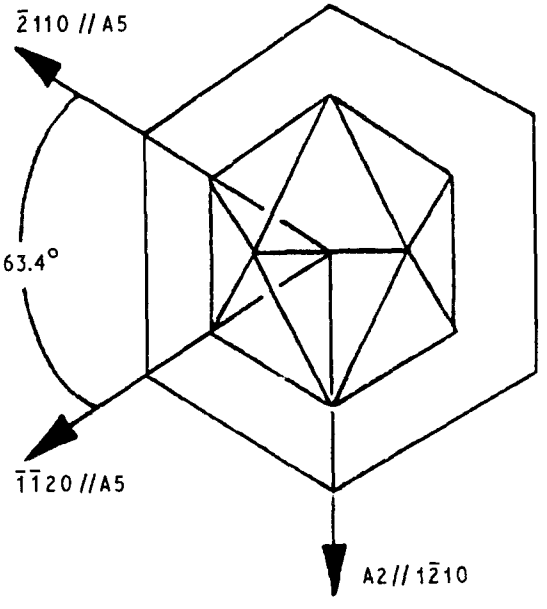

Figure 10 The Z–icosahedral interface and SAD pattern of two-fold icosahedral axis and $1\bar{2}10$ hexagonal zone axis.

3.3. Transformation behaviour

3.3.1. Differential scanning calorimetry

Both *in situ* hot-stage, and external heat treatments have been carried out to follow the decomposition behaviour of the icosahedral phase. DSC was used to determine heat-treatment temperature, the times involved for heat treatment, and the study of the transformations taking place. To determine the heat-treatment temperatures and times, a heating rate of 40 °C min^{-1} was used (this was the maximum rate possible, and was the closest approximation to the actual heating rate when the quartz tube was immersed in the saltpot).

In Fig. 11, the DSC curve is shown with all the (explainable) peaks marked. It has been suggested [39] that $Al_{51}Cu_{12.5}Li_xMg_{36.5-x}$ i-phases transform to the single b c c crystalline phase via an exothermic process, suggesting a metastable phase. After the exothermic reaction an endothermic reaction takes place at 524 °C. The exact nature of this reaction is not known but it has been suggested [3] that this reaction represents the transition from the b c c phase to an aluminium solid solution. This transformation, which was found to be reversible, has to be studied using a hot-stage X-ray experiment. Another unexplained peak was found at 548 °C. Finally, the largest endothermic peak represents the melting point. The icosahedral-to-hexagonal transition could not be identified on the DSC curve. From TEM investigations it is clear that the hexagonal phase appears simultaneously with the R-phase, its volume fraction being very low, however. This may indicate that the peak corresponding to the icosahedral-to-hexagonal transition is buried in the icosahedral-to-b c c peak.

The icosahedral to b c c transition temperature, the b c c to solid solution temperature, and the melting temperature were determined to be 419, 498 and 621 °C, respectively. In a previous experiment [3] (where a heating rate of 25 °C min^{-1} was employed) the i-phase to b c c transition to occur at 412 °C, and the b c c to solid solution transition to occur at 488 °C. The significant difference in temperatures can be accounted by the thermal lag resulting from the faster heating rate used in our study. The heats of transformation for the icosahedral to b c c, the b c c to solid solution, and the melting temperature are − 0.480, 19.354, and 152.043 J g^{-1}, respectively.

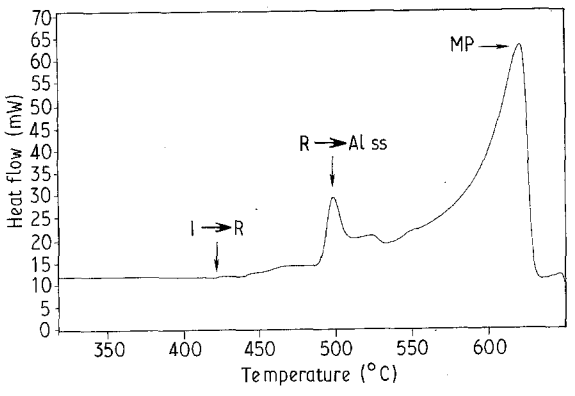

Figure 11 DSC curve of the transformation behaviour from 25–650 °C.

The isothermal treatments were done at 2 or 3 min intervals at 394 °C. The 20 min heat treatment corresponds to complete transformation.

3.3.2. Hot-stage experiment and general transformation behaviour

A bright-field image (Fig. 12) is shown of a sample which was held at 372 °C for 10 min. The image shows that the complete sample has transformed to the R-phase and no defects can be detected. Fig. 13 shows a sample which has undergone a temperature increase from room temperature to 350 °C in a 40 min period. Crystalline grains can be seen throughout the foil and it appears that the R-phase nucleates uniformly in the icosahedral matrix. CTEM experiments do not clearly show where the R-phase nucleates, although in some samples it seems to nucleate at the grain boundaries. It is possible that surface nucleation occurs in the hot-stage experiment thus giving results that do not represent the general nature of the transformation but are very specific to this hot-stage experiment.

Aluminium can be seen at grain boundaries and within icosahedral grains (see Fig. 14) in the ribbons which have been heat treated for short times. The reason aluminium is detected before the R-phase may be due to the following reasons: pre-existing nuclei found could be quenched-in aluminium, or aluminium (along with copper) which remained following sublimation of lithium and magnesium during heat treatment and/or melt spinning. Aluminium was the first phase identified upon heating and was found in all samples both within the icosahedral grains and on grain boundaries, but the size of the aluminium areas never exceeded 0.5 μm diameter. Upon progression of the reaction the aluminium areas do not seem to grow rapidly. The second phase that evolves is the R-phase. After annealing for 7 min the R-phase becomes the

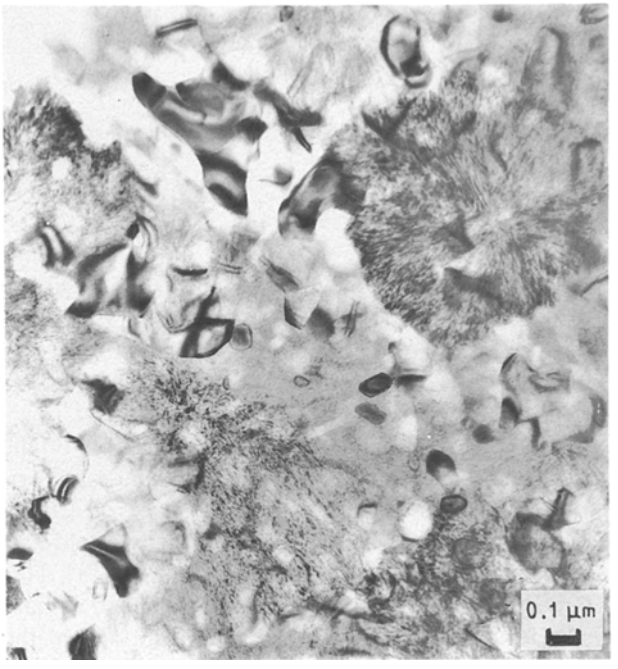

Figure 12 Hot-stage result at 372 °C for 10 min.

Figure 13 Hot-stage result of temperature increase from room temperature to 350 °C in 40 min.

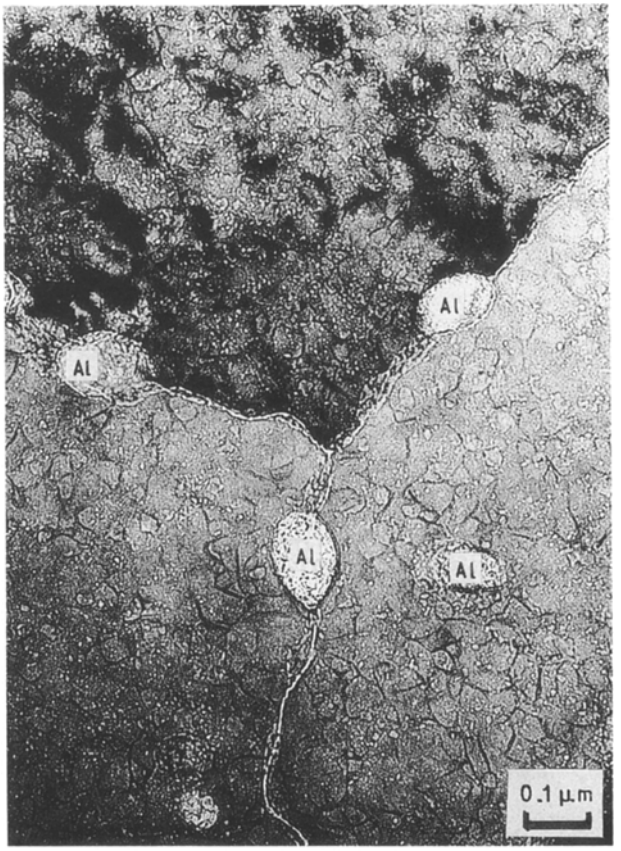

Figure 14 Bright-field micrograph showing aluminium nucleating in the icosahedral grains and on the boundaries.

majority phase. The Z-phase appears at the same time as the R-phase, though in smaller amounts. The Z-grains are usually completely surrounded by the R-grains.

4. Conclusions

The as-spun alloys consist of icosahedral grains which vary in diameter from 0.7–4.0 μm. The diffraction patterns of these icosahedral grains show distorted reflections. The quasilattice constant was determined to be 0.505 nm.

The quasicrystalline phase transforms during decomposition to three crystalline phases. The equilibrium b c c phase has a lattice parameter of 1.397 nm. The b c c phase was found to be closely related to the icosahedral phase because of the same chemical composition and a definite orientation relationship. A large number of planar defects was found in this phase on the $\{1\,1\,0\}$ and $\{1\,0\,0\}$ type planes.

The Z-phase, which was observed at the same time as the R phase, has lattice parameters of $a = 1.39$ nm and $c = 2.78$ nm. The grains of this phase were heavily faulted. The faults were found on $\{0\,0\,0\,1\}$ and $\{1\,1\,\bar{2}\,0\}$ planes. This phase has a structural relationship with the icosahedral phase but was compositionally found to be very different from both the icosahedral and R-phase.

The icosahedral to crystalline transformation occurs at 419 °C and the heat of transformation is -0.480 J g^{-1}. At the onset of the transformation aluminium appears, followed by the R-phase. The Z-phase appears with the R-phase but the volume fraction is significantly lower.

The R–icosahedral orientation relationship is expressed as $[0\,0\,1]\|[A_2]$, $[1\,1\,1]\|[A_3]$. $[\tau\,2\,0\,1]\|[A_3]$, $[1\,0\,\tau]$ and $[1\,\tau\,0]\|[A_5]$. The R- and Z-phases have a definite orientation relationship which can be expressed as $[0\,0\,1]\|[0\,0\,0\,1]$, $(0\,1\,0)\|(1\,0\,\bar{1}\,0)$. The Z- and icosahedral phases have a definite orientation relationship which results in the coincidence of four fivefold axes (all lying on the horizontal plane) with four $[1\,\bar{2}\,1\,0]$-type directions. The three orientation relationships were found to be self consistent.

Acknowledgements

The funding for this project was provided by the Department of Energy under grant number DE-FG05-89ER45389. We appreciate the useful discussions with Dr K. R. Lawless. Dr Y. Shen supplied the melt-spun ribbons. The ARM and the hot-stage experiment with the Kratos were performed at the National Center for Electron Microscopy, at LBL Berkeley.

References

1. D. SHECHTMAN, I. BLECH, D. GRATIAS and J. W. CAHN, *Phys. Rev. Lett.* **53** (1984) 1951.
2. C. SURYANARAYANA, S. CHANDRA and J. MENON, *J. Mater. Res.* **3** (1988) 34.
3. Y. SHEN, Thesis, University of Virginia (1988).
4. S. CHANDRA and C. SURYANARAYANA, *Phil. Mag. B* **58** (1988) 185.
5. A. L. MACKAY, *J. Phys. Paris* **47** (1986) C3-153.

6. H. K. HARDY and J. M. SILCOCK, *J. Inst. Metals* **24** (1955-56) 423.
7. E. E. CHERKASHIN, P. I. KRIPYAKEVICH, G. I. OLEKSIV, *Sov. Phys. Crystallogr.* **8** (1964) 681.
8. R. D. FIELD and H. FRASER, *Mater. Sci. Engng* **68** (1984–85) L17.
9. P. SAINFORT and B. DUBOST, *J. Phys. Paris* **47** (1986) C3-321.
10. W. A. CASSADA, G. J. SHIFLET and E. A. STARKE J, *Scripta Metall.* **20** (1986) 751.
11. P. SAINFORT, B. DUBOST and DABUS, *Compt. Rend. Acad. Sci. Paris* **301** (1985) 689.
12. B. DUBOST, J. M. LANG, M. TANAKA, P. SAINFORT and M. AUDIER, *Nature* **324** (1986) 48.
13. M. AUDIER and P. GUYOT, *J. Phys. Paris* **47** (1986) 405.
14. F. W. GAYLE, *J. Mater. Res.* **2** (1987) 1.
15. W. A. CASSADA, G. J. SHIFLET and S. J. POON, *Phys. Rev. Lett.* **56** (1986) 2276.
16. G. BERGMAN, J. L. T. WAUGH and L. PAULING, *Acta Crystallogr.* **10** (1957) 254.
17. M. AUDIER, J. PANNETIER, M. LEBLANC, C. JANOT, M. LANG and B. DUBOST, *Phys. B* **153** (1988) 136.
18. C. A. GURYAN, P. W. STEPHENS, A. I. GOLDMAN and F.W. GAYLE, *Phys. Rev. B* **37** (1988) 8495.
19. Y. SHEN, W. DMOWSKI, T. EGAMI, S. J. POON and G. J. SHIFLET, *ibid.* **37** (1988) 1146.
20. M. AUDIER, P. SAINFORT and B. DUBOST, *Phil. Mag. B* **54** (1986), L105.
21. Y. MA, E. A. STERN and F. W. GAYLE, *Phys. Rev. Lett.* **58** (1987) 1956.
22. W. DMOWSKI, T. EGAMI, Y. SHEN, S. J. POON and G. J. SHIFLET, *Phil. Mag. Lett.* **56** (1987) 63.
23. G. LAPASSET and A. LOISEAU, *J. Phys. Paris* **47** (1986) C3-489.
24. A. LOISEAU and G. LAPASSET, *Phil. Mag. Lett.* **56** (1987) C3-165.
25. *Idem, Phil. Mag. B* **56** (1987) L165
26. F. C. FRANK and J. S. KASPER, *Acta. Crystallogr.* **12** (1959) 483.
27. *Idem, ibid.* **11** (1958) 184.
28. A. LOISEAU and G. LAPASSET, *J. Phys. Paris* **47** (1986) C3-331
29. B. DUBOST, M. AUDIER, P. JEANMART, J. M. LANG and P. SAINFORT, *ibid.*. **48** (1987) C3-497
30. M. AUDIER, CH. JANOT, M. de BOISSIEU and B. DUBOST, *Phil. Mag. B* **60** (1989) 437.
31. K. F. KELTON and T. W. WU, *Appl. Phys. Lett.* **46** (1985) 1059.
32. A. J. DREHMAN, S. J. POON and K. R. LAWLESS, in "Rapidly Solidified Alloys and their Mechanical and Magnetic Properties", edited by B.C. Giessen, D. E. Polk, A. I. Taub Vol. 58 (Materials Research Society, Pittsburgh, PA, 1986) p. 249.
33. D. S. ZHOU, in Proceedings of the XII International Congress on Electron Microscopy", Seattle, Vol. 4 (1990) p. 456.
34. M. TANAKA, M. TERAUCHI and T. KANEYAMA, "Convergent Beam Electron Diffraction II" (Jeol Ltd, Tokyo, Japan).
35. V. ELSER, *Phys. Rev. B* **32** (1985) 4892.
36. T. C. LUBENSKY, J. E. S. SOCOLAR, P. J. STEINHARDT, P. A. BANCEL and P. A. HEINEY, *Phys. Rev. Lett.* **57** (1986) 1440.
37. V. ELSER, *Acta Crystallogr. A* **42** (1986) 36.
38. J. E. S. SOCOLAR and D. C. WRIGHT, *Phys. Rev. Lett.* **59** (1987) 221.
39. T. C. LUBENSKY, S. RAMASWAMY and J. TONER, *Phys. Rev. B* **33** (1986) 7715.
40. *Idem, ibid.* **32** (1985) 7444.
41. P. A. BANCEL, P. A. HEINEY, P. W. STEPHENS, A. I. GOLDMAN and P. M. HORN, *Phys. Rev. Lett.* **54** (1985) 2422.
42. C. SURAYANARAYANA and H. JONES, *Int. J. Rapid Solid.* **3** (1987) 253.
43. G. J. SHIFLET, Q. B. YANG, D. S. ZHOU and S. J. POON, *Phil. Mag. A*, **64** (1991) 483.
44. Q. B. YANG, D. S. ZHOU and G. J. SHIFLET, *Phil. Mag. A*, **65** (1992) 1395.
45. V. ELSER and C. L. HENLEY, *Phys. Rev. Lett.* **55** (1985) 2883.
46. M. DUNEAU and A. KATZ, *ibid.* **54** (1985) 2688.
47. J. M. LEGRESEY, M. AUDIER, J. P. SIMON and P. GUYOT, *Acta Metall* **34** (1986) 1759.
48. W. A. CASSADA, Thesis, University of Virginia (1987).
49. D. C. KOSKENMAKI, H. S. CHEN and K. V. RAO, *Phys. Rev. B* **33** (1986) 5328.

Received 30 September 1991
and accepted 11 June 1992